Functional Profiling of L-Alanine Diglycine Picrate (LADGP) Single Crystal for Nonlinear Optical Enhancement

R. Suganthi¹, Dr. K.Balasubramanian^{2*}

¹ Research scholar (Reg.No:21211072132002), PG &Research Department of Physics, The M.D.T. Hindu college, Pettai, Tirunelveli -627010, Tamilnadu , India.

^{2*}Associate Professor, PG & Research Department of Physics, The M.D.T. Hindu college, Pettai, Tirunelveli-627010, Tamilnadu, India.

Affiliated^{1,2*} by Manonmanium Sundaranar University, Abishekapatti-627012, Tirunelveli, Tamilnadu, India.

Abstract: The L-Alanine Diglycine Picrate (LADGP) single crystal was cultivated employing the slow evaporation solution method under usual atmospheric conditions. The structural confirmation for the LADGP crystalline material was conducted via single crystal X-ray diffraction (SXRD), revealing a monoclinic structure having the P2₁/n space symmetry. The powder X-ray diffraction (PXRD) was utilized for ascertaining the crystalline structure of the LADGP crystal. Vibrational assignments and identification of functional moieties of the LADGP single crystal were achieved through Fourier Transform Infrared spectroscopy. Microhardness measurements were performed to probe the mechanical robustness of the LADGP crystal, highlighting its exceptional durability. The optical qualities in the LADGP crystal were evaluated with UV-visible near-infrared spectroscopy. Electrical properties of LADGP crystal were investigated through conducting dielectric experiments (constant and loss) as a varying with frequency at three different temperature. The photoconductivity measurements showed that the LADGP crystal becomes more conductive when exposed to different types of light. The LADGP crystal exhibited a laser damage threshold (LDT) of 2.6 GW/cm², suggesting its aptness for laser-related uses. The nonlinear third-order susceptibility was assessed and analyzed using Z-scan techniques.

Keywords: Crystal growth, SXRD, PXRD, FTIR, Microhardness, UV-vis-NIR, Dielectric, LDT and Z-scan analysis.

1. Introduction

In recent times, complex organic crystals encompassing salts and co-crystals have gained significant importance in optoelectronics, chemical sciences, and biological sciences. This is owing to their swift responsiveness and the diffusion of electrons at the molecular scale[1]. Organic crystals exhibit built-in flexibility in synthesis, greater nonlinear coefficients, wide transparency, and favourable dielectric behavior in contrast to inorganic materials. By selecting versatile component molecules and harnessing intermolecular collisions like classical and non-classical hydrogen bonding, unique physicochemical properties can be achieved in co-crystals and salts during their formation [2].

One of the primary benefits of organic materials is their capability to undergo structural alterations to achieve desired nonlinear optical (NLO) properties. L-Alanine, the simplest amino acid after glycine, is water-soluble and adept at reacting with acids to create new NLO compounds. Diglycine picrate has been identified in several research papers as a potential NLO material [3-4].

In this particular study, L-Alanine was combined with Diglycine picrate to synthesize L-Alanine diglycine picrate. Various analyses, covering SXRD, Powder XRD, FTIR-spectroscopy, Microhardness testing, UV-visible-near infrared spectroscopy, dielectric analysis, laser damage threshold assessment, and Z-scan investigation, were conducted and discussed for the first time.

2.Experimental Details

2.1Growth and synthesis procedure

The synthesis of the LADGP compound involved utilizing the slow evaporation solution method, where L-Alanine and Diglycine picrate were incorporated at a 1:1 molar ratio. Initially, specific amounts of both substances were solubilized separately in distilled water, each in its own beaker. Once dissolved, the solutions were gradually combined and stirred thoroughly for 8 hours at room temperature to ensure complete reaction. The resulting solution exhibited a yellow hue, indicating successful chemical transformation. Subsequently, the solution was permitted to evaporate naturally at ambient conditions, resulting in the formation of yellow crystalline LADGP salt. The well-developed LADGP single crystal, sized at 9 mm \times 8 mm \times 5 mm was cultivated over a development duration of 14 days. Figure 1 illustrates the resulting LADGP single crystal.

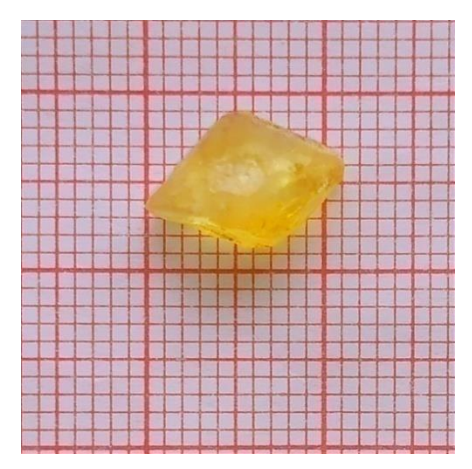


Figure.1 A picture of LADGP single crystal

2.2 Characterization techniques:

The LADGP crystal underwent comprehensive analysis using advanced instrumentation across various disciplines: single crystal XRD employed a BRUKKER AXS (kappa APEXII) diffractometer utilizing graphite monochromated MoK α radiation (λ =0.71071 Å). The powder XRD was executed employing a BRUKKER D8 ADVANCE instrument. The vibrational assignments in the 400–4000 cm⁻¹ range were ascertained via a BRUKER AXS FTIR Spectrometer. Vickers microhardness testing utilized a SHIMADZU-HMV-G21model tester featuring a diamond-tipped indenter. UV-visible analysis employed a JASCO-V-730 Spectrometer. Dielectric analysis was performed using an Agilent E 4980A LCR Z meter spanning a frequency spectrum of 50 Hz to 2 MHz. The investigation into photoconductivity utilized a Keithley picoammeter instrument (MODEL M6487). Laser damage threshold investigations utilized a Q switched Neodymium-Yttrium Aluminum Garnet laser at 1064 nanometres of the Quanta Ray type. The nonlinear susceptibility value was derived via Z-scan analysis, employing a steady laser beam (21 mW) at 632.8 nanometers.

3. Results and Discussion

3.1 X-ray Diffraction for Structural Elucidation

Single crystal X-ray diffraction investigation involves directing X-rays at a crystal to precisely determine its atomic structure, offering valuable insights into its composition and arrangement at the atomic level. This technique is indispensable for acquiring an in-depth comprehension of the fundamental properties and behaviors of materials [5]. The lattice parameters for LADGP are as specified: a=5.10Å, b=11.95Å, c=5.45 Å, $\alpha=90^{\circ};\beta=111.67^{\circ};\gamma=90^{\circ}$ with a V=309(Å)³. These values imply that the LADGP crystal classified under the monoclinic structure, specifically in the centrosymmetric space symmetry P2₁/n. Table 1 presents the single crystal XRD (SXRD) data pertaining to the DGP and LADGP crystals. Various diffraction planes and phase purity are detected through powder XRD analysis. The measurements are conducted across a 2θ degree span from $10^{\circ}-50^{\circ}$ at ambient temperature. From the resulting graph, the maximum intensity was observed at an angle

of 29.886°. The existence of high sharp peaks points to the quality of the crystalline structure of the LADGP crystal. The PXRD spectra of LADGP are illustrated in figures 2(a) and 2(b). Additionally, the powder XRD data of LADGP are provided in table 2.

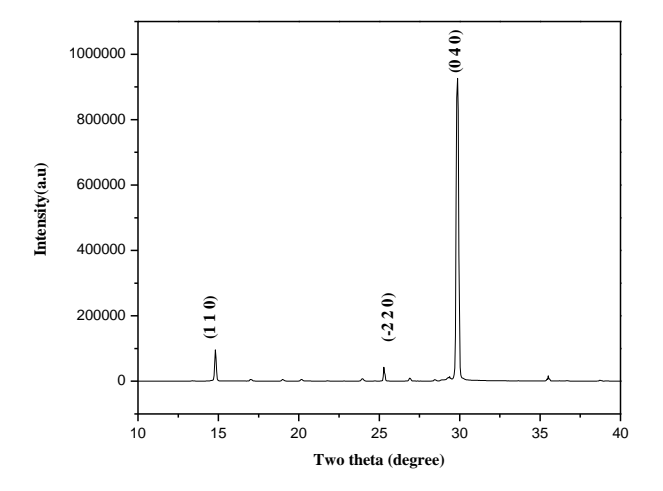
Table 1. SXRD data for DGP and LADGP crystal

Crystal Name	Lattice	Volume (Å) ³	Z
	parameters		
Diglycine Picrate (DGP)	a=15.142Å b=6.654 Å c=15.367 Å α =90°; β =93° γ =90°	1541.47	2
L-Alanine Diglycine Picrate (LADGP)	a= 5.10\AA b= 11.95\AA c= 5.45 Å $\alpha=90^{\circ}$; $\beta=111.67^{\circ}$ $\gamma=90^{\circ}$	309	4

Table 2.PXRD details about LADGP crystal

Pos.[°2Th.]	Height[cts]	d spacing[Å]	Rel.int.[%]	hkl
15.682	4096.71	6.02849	0.5	1 1 0
25.348	3.5109	3.5109	2.6	-2 2 0
29.886	2.98726	2.98726	100	0 4 0

Figure.2a).XRD pattern of LADGP with hkl indices



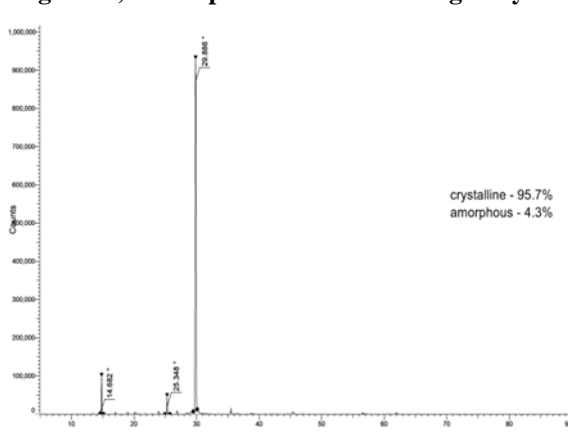


Figure2b) XRD spectra of LADGP single crystal

3.2 Fourier Transform Infrared Spectroscopy

FTIR spectroscopy in crystals enables precise analysis of their molecular structure, aiding in identifying chemical bonds, lattice vibrations, and defects. It's instrumental in characterizing crystal quality, understanding crystal growth mechanisms, and optimizing material properties for diverse applications like electronics and photonics [6-7]. FTIR spectroscopy serves as a crucial method for identifying assorted functional groups and molecular interactions present in samples. The FTIR spectrum of LADGP, obtained within the 1000-4000 cm⁻¹ range utilizing the KBr pellet method, is depicted in figure 3. The broad-spectrum span was identified in the range of 1600-3200cm⁻¹ as seen in figure.3. The absorption bands in the spectrum are assigned based on IR spectral data, with the corresponding assignments of vibrational modes are detailed in table 3.

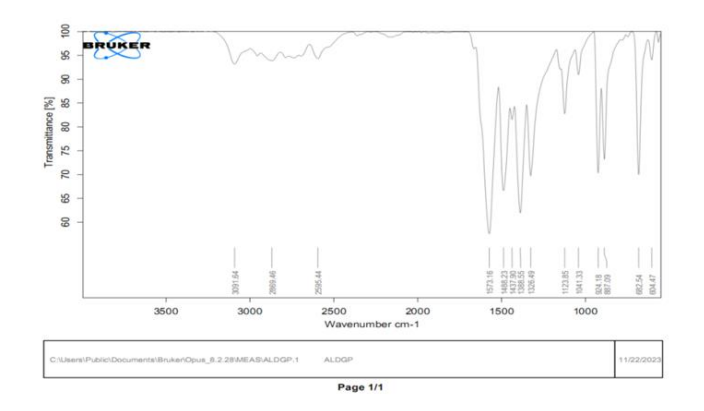


Figure 3. FTIR spectrum for LADGP

Table 3: FTIR Spectral Profiles of LADGP

Wave Number (cm		
1)	Assignment modes	Compound
3091.64	C-H stretching	Alkene
2869.46	N-H stretching	Amine salt
2595.44	O-H stretching	Carboxylic acid
1573.16	C-H bending	Aromatic compound
1488.23	N-O stretching	Nitro group
1437.9	N-O stretching	Nitro group
1388.55	C-H bending	Aldehyde

1326.49	N-O stretching	Nitro group
1123.85	C-O stretching	Secondary alcohol
1041.33	C-O-CO stretching	Stretching anhydride
924.18	C-H bending	1,2,4tri substituitional
887.09	C=C bending	alkene

3.3 Microhardness Analysis

Desirable hardness behavior in crystals denotes their capacity to withstand deformation and penetration, highlighting their strong structural integrity and long-lasting durability. Crystals exhibiting such behavior are suitable for applications requiring high mechanical strength and resistance to abrasion [8]. The microhardness value is subsequently determined through the following formula,

$$H_v = 1.8544 \text{ P/d}^2 \text{ kg/mm}^2$$

Here ' H_v ' denotes the hardness value, 'P'represents the applied load in kilograms, and 'd' is the average diagonal measurement of the indentation in millimeters. Figure 4(a) presents a plot showing the relationship of the logarithms of 'P' and 'd'. The measured value of n (B=0.26354) on the graph confirms that the LADGP crystal falls within the hard category [9]. In figure 4(b), a graphical representation demonstrates the correlation of the hardness number 'Hv' and the applied load 'P. Examining the plot reveals that the weight increases from 25g to 50g, the hardness value (Hv) exhibits a linear increase with the load, whereas beyond 50g, Hv rises steadily. The hardness value obtained from the grown LADGP crystal indicates a need for higher stress to induce micro damages, affirming its superior crystalline perfection [10]. This quality makes the crystal highly suitable for device fabrication purposes.

Fig.4a) variation of log P against log d

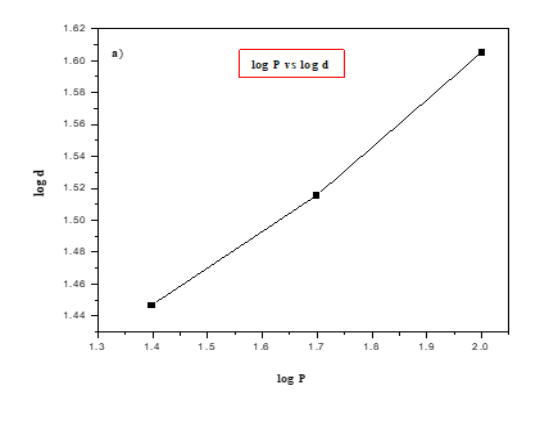
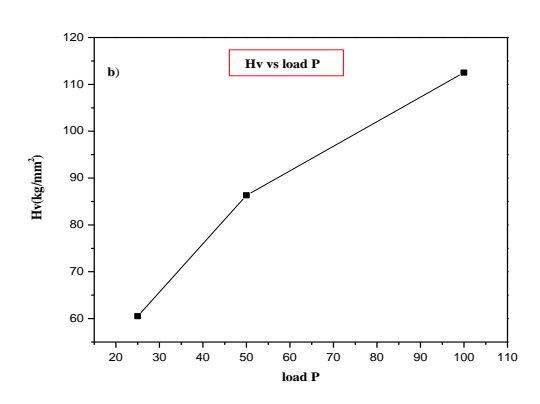


Fig.4b) variation of Hv against load P

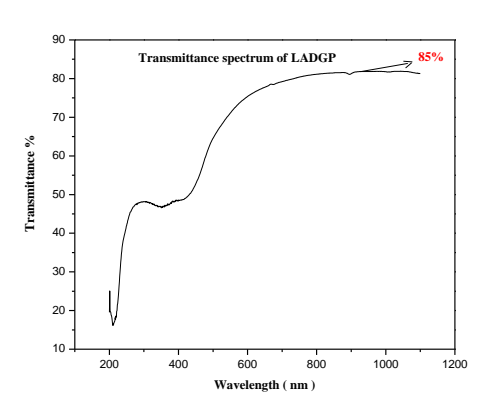


3.4 UV-vis NIR Evaluation

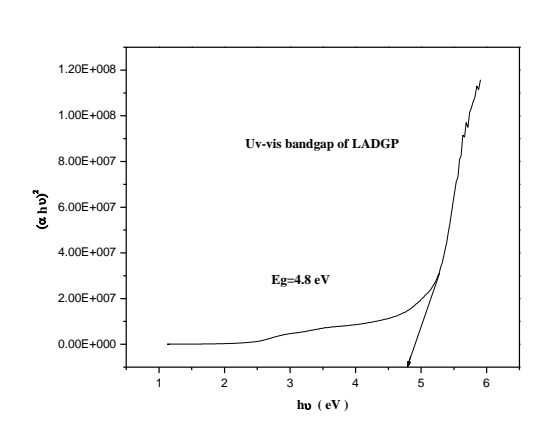
UV spectroscopy is crucial for crystal analysis, as it explores the electronic transitions within the material. By interacting with crystals, UV light reveals valuable insights into their electronic structure, optical characteristics, and potential uses in diverse fields like materials science, semiconductor technology, and photovoltaics [11]. The optical transmittance graph for the LADGP single crystal is manifested in figure 5(a). The LADGP crystal boasts an 85% transmittance rate, with a broad window extending from 410 to 1100 nm, offering considerable advantages for a multitude of optical applications. Throughout the UV-visible NIR spectrum, LADGP crystal exhibits commendable transmission and minimal absorption. Figure 5(b) reveals the (α hv) vs (hv) plot, serving to elucidate the forbidden energy gap spectrum. By extrapolating from the linear segment of the curve, an optical band gap value of 4.8 eV is discerned for LADGP crystal. Additionally, Figure 5(c) exhibits the absorption curve of LADGP single crystal, revealing lower cut-off wavelengths observed at 210 and 380 nm. These absorption features are attributed to specific transitions, namely the n- σ * and σ - σ * transitions within the LADGP single crystal [12]. The optical response of the LADGP crystal demonstrates a distinct trend of

increasing optical conductivity at a specific wavelength of 350 nm, as illustrated in Figure 5(e) displays the variation of refractive index with wavelength, revealing a lower refractive index of 0.025 in the perceptible region for the LADGP crystal. As the wavelength of light increases, there is a corresponding reduction in the refractive index of LADGP crystal. The LADGP crystal's extinction coefficient alters with different wavelengths, as seen in figure 5(f). The extinction coefficient directly corresponds to the absorption coefficient for the LADGP single crystal. At wavelengths of 280 nanometers in the UV region and 550 nanometers in the visible region, the extinction coefficient reaches its minimum value, which causes a decrease in light absorption at these specific wavelengths. Thus, the LADGP crystal wider band gap, lower refractive index, and consistent transmission throughout the spectrum make it well-suited for advanced optoelectronic applications.

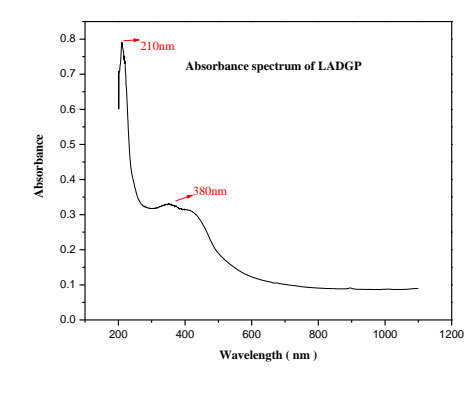
5a) Transmittance versus wavelength



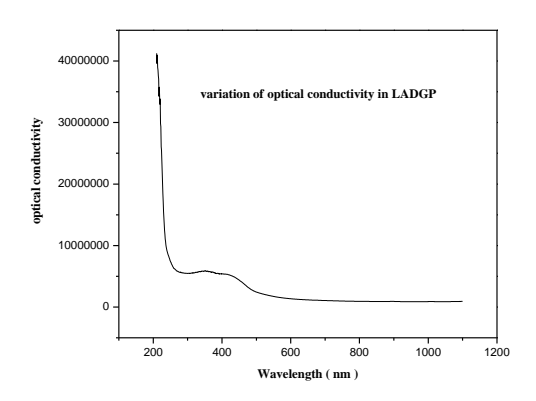
5b) Tauc plot of LADGP



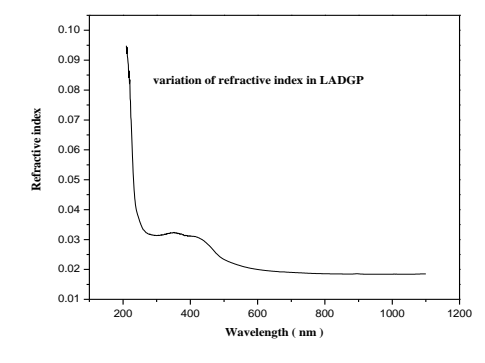
5c) Absorbance versus wavelength



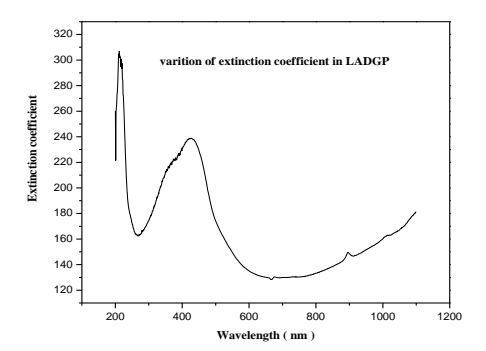
5d) Optical conductivity versus wavelength



5e) Refractive index versus wavlength



5f) Extinction coefficient versus wavelength



3.5 Dielectric study

A dielectric study on crystals involves examining the behavior of crystals in response to an applied electric field. This study aims to understand how crystals interact with electric fields and how their dielectric properties, such as permittivity and conductivity, are influenced by numerous factors like crystal structure, defects, temperature, and the applied field frequency. Dielectric loss points to the dissipation of energy as heat within a dielectric material when exposed to a varying electric field. Dielectric constant, quantifies a material's capacity to store electrical energy when affected by an electric field, reflecting its permittivity relative to a vacuum [13].

Dielectric analysis was conducted on LADGP single crystal to assess its dielectric properties (permittivity & loss) over frequencies that varied from 1 Hz to 1 MHz, encompassing temperatures of 30°C, 50°C, 70°C. Figures 6(a) and 6(b) portray the correlation between the dielectric constant and loss in the LADGP crystal. Figure 6(a) demonstrates a significant dielectric constant value across a diminished range of frequencies at all temperatures, possibly stemming from occurrence of diverse polarizations—ionic, electronic, space charge, and orientation [14].

The reduction in dielectric constants at elevated frequencies is attributable to the deficiency of space charge polarization around the interfacial region between grains. In figure 6(b), the minimal dielectric loss (tan δ) observed for all temperatures in the LADGP single crystal highlights its superior optical quality, characterized by few defects, making it highly suitable for applications in nonlinear optics (NLO). In figure 6(c), it is clearly depicted that with rising frequency, the AC conductivity also escalates in the LADGP single crystal. Materials with AC conductivity that increases with frequency can significantly enhance the performance and efficiency of nonlinear optical devices and applications. Table 4.presents the activation energy values for LADGP.

Fig.6a) dielectric constant in LADGP

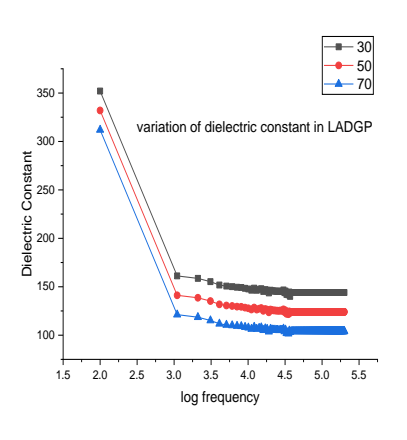


Fig.6b) dielectric loss in LADGP

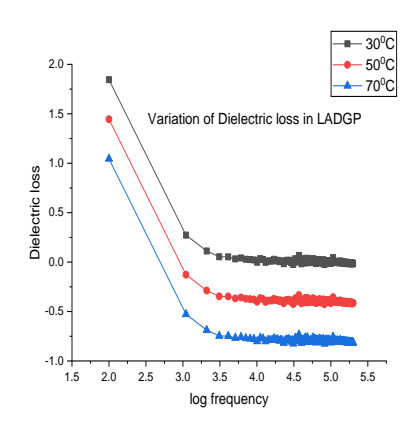
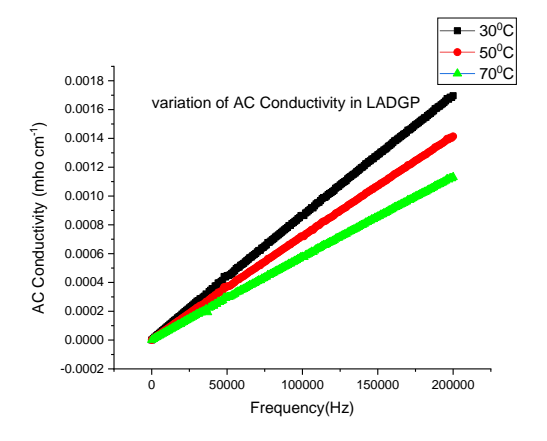


Fig.6c) AC conductivity in LADGP



Frequency(Hz)	Ea/K	in eV
100	31.8256	0.0027424
1099	12.2159	0.0010526
10095	3.956	0.0003409
50075	3.556	0.0003064
100050	2.75	0.000237
200000	2.55	0.0002197

3.6 Photoconductivity study

Photoconductivity studies on crystals provide essential insights into their electronic and optical behaviors. These investigations explore how crystals produce and transfer charge carriers under light exposure, crucial for optimizing the efficiency of electronic devices. Advanced material characterization methods, including spectroscopy and microscopy, are employed to unravel the impact of crystal structure and composition on photoconductivity. This understanding is pivotal for optimizing device performance and exploring new applications in electronic and photonic technologies [15-17]. At ambient temperature, the photoconductivity of the LADGP crystal was examined. Dark current measurements were taken incrementally from 0 to 50 Volts without exposure to radiation, while photocurrent was measured under halogen lamp illumination at 100 Watts. Figure.7 illustrates the relationship between I_p and I_d across varying applied voltages. The LADGP crystal demonstrates positive photoconductivity, indicated by I_p surpassing I_d , likely attributable to photon absorption generating mobile charge carriers. The LADGP crystal's photosensitivity was assessed using a specific equation [18],

Photo sensitivity,
$$S = \frac{I_p - I_d}{P}$$

Here, 'I_p' is the photocurrent, 'P' is the incident optical power, 'I_d' is the dark current. The positive photoconductivity of LADGP crystal drives high-performance displays and sensors with rapid response and low noise, advancing light-induced conductivity technologies [19].

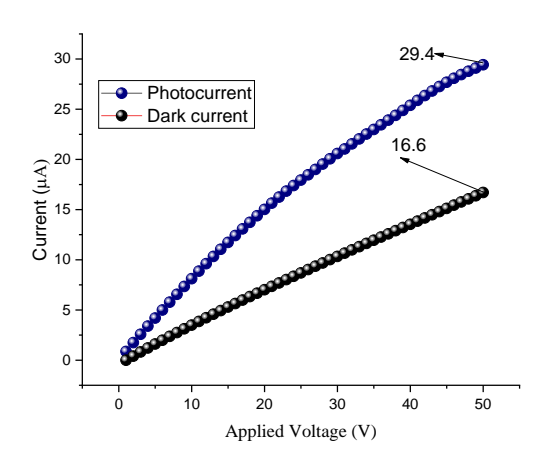


Fig.7 Photoconductivity for LADGP crystal

3.7 Laser Damaged Threshold (LDT) study

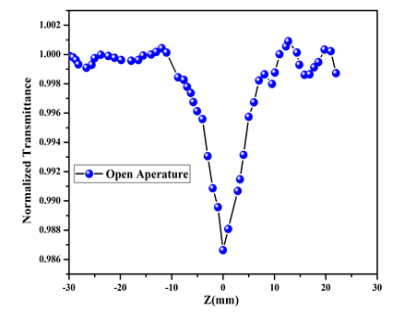
A laser damage threshold study on crystals involves investigating the point at which a crystal material begins to deteriorate or sustain irreversible damage when exposed to intense laser radiation. This research aims to

understand the limits of a crystal's resilience to high-energy photon interactions, crucial for various applications such as laser technology, optics, and materials science [20-21]. The investigation into the Laser damage threshold involved subjecting the LADGP crystal to a high-energy Neodymium-doped Yttrium Aluminum Garnet laser functioning at 1064 nanometer wavelength in a Q-switched configuration. A pulse duration of 6 nanoseconds was employed, and the laser irradiation, set at 1064 nm, was directed towards the LADGP sample at a frequency of 10 Hz. The incident laser light was focused with a 10 cm focal length. The laser light's pulse energy was guaged with a power meter, and the energy density was computed utilizing the specified expression [22], Power density, $P_d = E/\tau \pi r^2$

In this equation, 'E' stands for the energy density input measured in millijoule (mJ), 'τ' signifies the pulse width expressed in nanosecond (ns), and 'r' indicates the spot's radius in millimeter (mm). Notably, the LADGP crystal shows an impressive laser damage threshold of 2.6 GW/cm², surpassing that of KDP (0.20 GW/cm²) and Urea (1.50 GW/cm²). This characteristic highlights the LADGP crystal's exceptional optical damage tolerance [23], making it a promising prospect for integration into high-energy laser devices.

3.8 Z-Scan Investigation

The investigation into the third order nonlinear optical (NLO) characteristics of LADGP single crystal was conducted utilizing the Z-scan approach. A polarized Gaussian laser light with TEM00 mode was passed into a convex lens having a focal length of 200 millimeters, producing a beam diameter (ω_0) of 16.1µm for LADGP. The sample's thickness (L) measured 1 mm, with a calculated Rayleigh length (ZR) of 1.3 mm. It was observed that when (L<ZR), with the negative (-Z) to positive (Z) axis aligned along the path of the laser light, the condition was satisfied [24-26]. The computer-controlled translation of the sample holder was monitored, and the electronic power meter recorded the transmitted intensity accordingly at each instance. Using a closed aperture, the signal intensity varied depending upon the aperture size (2 millimeters in diameter). Conversely, with an open aperture, the intensity was compiled by the sensor to ascertain the nonlinear absorption coefficient (β). The laser light's strength was found to be significantly affected by both the refractive index of samples and the absorption properties of those materials. In closed-aperture configuration, the non-linear third order refractive index 'n₂' value was measured at 2.92503×10⁻¹² m²/W for LADGP single crystal. Figure 7(a) illustrates reverse saturable absorption, as evidenced by the peak intensity at the focal point (Z=0) in the open aperture configuration. Conversely, Figure 7(b) demonstrates a transition from valley to peak in the closed aperture configuration, indicating a self-focusing effect induced by the sample [27-29]. Under the open aperture configuration, the absorption coefficient 'B' scrutinized as 9.2217×10⁻⁵ m/W for LADGP single crystal. The magnitude of the third order susceptibility $'\chi^{(3)'}$ recorded at 3.8189×10⁻⁸ esu for LADGP. The presence of a positive nonlinear refractive index (n₂) signifies that the material exhibits self-focusing characteristics [30]. The self-focusing nature of LADGP single crystal, opens up a wide range of opportunities for applications in optics, photonics, and materials science, with potential implications in areas such as telecommunications, laser technology and biomedical imaging.



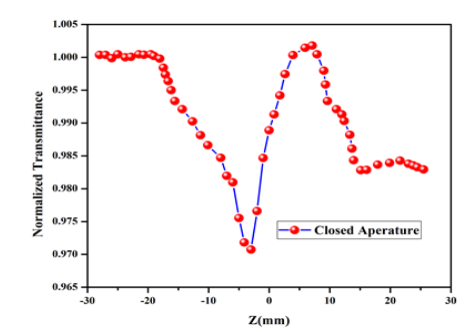


Fig.8 (a) open aperture spectrum of LADGP

Fig.8(b) closed aperture spectrum of LADGP

4.Conclusion

A high-quality monolithic crystal of LADGP was cultivated employing the slow evaporation solution method, yielding in a transparent yellow crystal measuring 9 x 8 x 5 mm³ in dimensions. The lattice arrangement of LADGP, ascertained via single crystal XRD, falls under the monoclinic structure, specifically within the centrosymmetric space symmetry $P2_1/n$. The purity in the LADGP crystal was validated through Powder XRD investigation. Functional groups and their vibrations underwent examination using FTIR evaluation. The hardness characteristics in the LADGP crystal were assessed via Vicker microhardness test. UV-Vis-NIR spectroscopy revealed a favorable optical transparency of 85% in the LADGP crystal, with cut-off wavelengths at 210 and 353 nm, exhibiting its suitability for Nonlinear Optical (NLO) device utilizations. The LADGP crystal showcased excellent optical quality, with a low dielectric loss at high frequencies, as evidenced by its dielectric response. The photoconductivity measurements indicate that LADGP exhibits a positive response to light-induced conductivity. The laser damage threshold for the LADGP crystal, estimated at 2.6 GW/cm², indicates its strong suitability for laser applications. Furthermore, the susceptibility ($\chi^{(3)}$) value for the LADGP crystal was determined as 3.8189×10⁻⁸ esu, affirming its suitability for practical devices such as remote sensing and lighting control.

References

- [1] S. Sivaraman, C. Balakrishnan, A. A. Prasad, R. M. Sokalingam, S. P. Meenakshisundaram, & R. Markkandan. Crystal growth, structure and characterization of diglycine zinc dipicrate: Centrosymmetric crystal exhibiting second harmonic generation efficiency. Molecular Crystals and Liquid Crystals, 656(1), 153-168 (2017).
- [2] C. Razzetti, M. Ardoino, L. Zanotti, M. Zha, & C. Paorici. Solution growth and characterisation of L-alanine single crystals. Crystal Research and Technology: Journal of Experimental and Industrial Crystallography, 37(5), 456-465 (2002).
- [3] M. Shkir, S. Muhammad, S. AlFaify, A. Irfan, M. A. Khan, A. G. Al-Sehemi, & I. Bdikin. A comparative study of key properties of glycine glycinium picrate (GGP) and glycinium picrate (GP): A combined experimental and quantum chemical approach. Journal of Saudi Chemical Society, 22(3), 352-362 (2018).
- [4] V. V. Ghazaryan, M. Fleck, & A. M. Petrosyan. Glycine glycinium picrate—Reinvestigation of the structure and vibrational spectra. Spectrochimica Acta Part A: Molecular and Biomolecular Spectroscopy, 78(1), 128-132 (2011).
- [5] N. Vijayan, S. Rajasekaran, G. Bhagavannarayana, R. Ramesh Babu, R. Gopalakrishnan, M. Palanichamy, & P. Ramasamy. Growth and characterization of nonlinear optical amino acid single crystal: L-alanine. Crystal Growth & Design, 6(11), 2441-2445 (2006).
- [6] D. Shanthi, P. Selvarajan, & R. J. Mani. Nucleation kinetics, growth and hardness parameters of 1-alanine alaninium picrate (LAAP) single crystals. Optik, 125(11), 2531-2537 (2014).
- [7] K. D. Parikh, D. J. Dave, B. B. Parekh, & M. J. Joshi. Growth and characterization of L-alanine doped KDP crystals. Crystal Research and Technology: Journal of Experimental and Industrial Crystallography, 45(6), 603-610 (2010).
- [8] S. Varughese, M. S. R. N. Kiran, U. Ramamurty, & G. R. Desiraju. Nanoindentation in crystal engineering: quantifying mechanical properties of molecular crystals. Angewandte Chemie International Edition, 52(10), 2701-2712 (2013).
- [9] G. Shanmugam, & S. Brahadeeswaran. Spectroscopic, thermal and mechanical studies on 4-methylanilinium p-toluenesulfonate—a new organic NLO single crystal. Spectrochimica Acta Part A: Molecular and Biomolecular Spectroscopy, 95, 177-183 (2012).
- [10] C. M. Reddy, G. R. Krishna, & S. Ghosh. Mechanical properties of molecular crystals—applications to crystal engineering. CrystEngComm, 12(8), 2296-2314 (2010).
- [11] R. Hanumantharao, & S. Kalainathan. Growth and spectroscopic investigation of a new crystal for NLO applications: C10H20KN5O9. Spectrochimica Acta Part A: Molecular and Biomolecular Spectroscopy, 99, 181-188 (2012).

- [12] K. Ambujam, S. Selvakumar, D. Prem Anand, G. Mohamed, & P. Sagayaraj. Crystal growth, optical, mechanical and electrical properties of organic NLO material γ-glycine. Crystal Research and Technology: Journal of Experimental and Industrial Crystallography, 41(7), 671-677 (2006).
- [13] E. D. D'silva, G. K. Podagatlapalli, S. V. Rao, & S. M. Dharmaprakash. Structural, optical and electrical characteristics of a new NLO crystal. Optics & Laser Technology, 44(6), 1689-1697 (2012).
- [14] P. L. Mageshwari, R. Priya, S. Krishnan, V. Joseph, & S. J. Das. Growth, optical, thermal, dielectric and mechanical studies of sodium hydrogen succinate single crystal: a third-order NLO material. Journal of Thermal Analysis and Calorimetry, 128, 29-37 (2017).
- [15] C. M. Ngue, K. F. Ho, B. Sainbileg, E. Batsaikhan, M. Hayashi, K. Y. Lee, ... & M. K. Leung. Conductivity and photoconductivity in a two-dimensional zinc bis (triarylamine) coordination polymer. Chemical Science, 14(5), 1320-1328 (2023).
- [16] K. W. Böer & U. W. Pohl. Photoconductivity. *In* Semiconductor Physics (pp. 1299-1324). Cham: Springer International Publishing (2023).
- [17] R. Purusothaman, M. Shankar, A. Dennis Raj, M. Vimalan, & I. Vetha Potheher. A study on NLO, ultraviolet transparency, photoconductivity, and dielectric response of organic single crystal. Journal of Materials Science: Materials in Electronics, 34(36), 2292 (2023).
- [18] R. Akiyoshi, A. Saeki, K. Ogasawara, & D. Tanaka. Impact of substituent position on crystal structure and photoconductivity in 1D and 2D lead (ii) benzenethiolate coordination polymers. Journal of Materials Chemistry C, 12(6), 1958-1964 (2024).
- [19] B. Zhao, H. Chen, R. Ahsan, F. Hou, E. R. Hoglund, S. Singh, ... & J. Ravichandran. Photoconductive Effects in Single Crystals of BaZrS3. ACS Photonics, 11(3), 1109-1116 (2024).
- [20] T. Suresh, S. Vetrivel, S. Gopinath, & E. Vinoth. Investigation on synthesis, laser damage threshold, and NLO properties of 1-asparagine thioacetamide single crystal for photonic device applications. Journal of Materials Science: Materials in Electronics, 31, 13310-13320 (2020).
- [21] P. Karuppasamy, M. S. Pandian, P. Ramasamy, & S. Verma. Crystal growth, structural, optical, thermal, mechanical, laser damage threshold and electrical properties of triphenylphosphine oxide 4-nitrophenol (TP4N) single crystals for nonlinear optical applications. Optical Materials, 79, 152-171 (2018).
- [22] T. D. Rani, M. Rajkumar, & A. Chandramohan. Synthesis, crystal structure, thermal, mechanical and laser damage threshold studies of an NLO active organic molecular adduct: 4-Acetylpyridine: 4-aminobenzoicacid. Materials Letters, 222, 118-121 (2018).
- [23] Z. S. Shanon, & R. Sh. Study of the Nonlinear Optical Properties of Lithium Triborate Crystal by Using Z-Scan. International Journal of Science and Research (IJSR), 1683 (2016).
- [24] B. Mohanbabu, R. Bharathikannan, & G. Siva. Structural, optical, dielectric, mechanical and Z-scan NLO studies of charge transfer complex crystal: 3-aminopyridinum-4-hydroxy benzoate. Journal of Materials Science: Materials in Electronics, 28, 13740-13749 (2017).
- [25] V. Natarajan, T. Sivanesan, & S. Pandi. Third order non-linear optical properties of L-arginine hydrochloride monohydrate single crystals by Z-scan technique. Indian Journal of Science and Technology, 897-899 (2010).
- [26] T. Thilak, M. B. Ahamed, & G. Vinitha. Third order nonlinear optical properties of potassium dichromate single crystals by Z-scan technique. Optik, 124(21), 4716-4720 (2013).
- [27] V. Natarajan, T. Sivanesan, & S. Pandi. Third order non-linear optical properties of potassium aluminium sulphate single crystals by Z-scan technique. Indian J. Sci. Technol, 3(6), 656-658 (2010).
- [28] Z. Lian, N. Zhao, P. Liu, C. An, A. Wang, & F. Yang. Crystal structures and investigation of the third-order nonlinear optical properties of four coordination polymers by using the Z-scan technique. CrystEngComm, 20(38), 5833-5843 (2018).
- [29] A. T. Ravichandran, R. Rathika, & M. Kumaresavanji. Growth and Z-scan analysis of semi-organic Bis (picolinic acetate) Zinc (II) single crystal for third order NLO applications. Journal of Molecular Structure, 1224, 129048 (2021).
- [30] M. Parishani, M. Nadafan, & R. Malekfar. Z-scan investigation to evaluate the third-order nonlinear optical properties of cauliflower-like VS 2 structures. JOSA B, 38(5), 1586-1592 (2021).